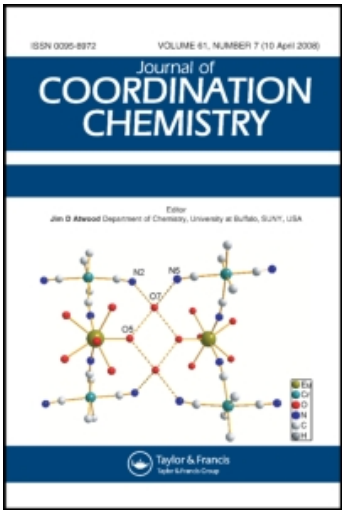

Journal of Coordination Chemistry
Publication details, including instructions for authors and subscription information:
http://www.informaworld.com/smpp/title~content=t713455674

Synthesis, crystal structure, and DNA binding of a new oxalato-bridged binuclear zinc(II) complex

Wei Sun[a]; Man Jiang[a]; Yan-Tuan Li[a]; Zhi-Yong Wu[a]; Wei-Bing Peng[a]
[a] Marine Drug and Food Institute, Ocean University of China, Qingdao, Shandong 266003, P.R. China

To cite this Article Sun, Wei , Jiang, Man , Li, Yan-Tuan , Wu, Zhi-Yong and Peng, Wei-Bing(2009) 'Synthesis, crystal structure, and DNA binding of a new oxalato-bridged binuclear zinc(II) complex', Journal of Coordination Chemistry, 62: 15, 2520 — 2531
To link to this Article: DOI: 10.1080/00958970902846126
URL: http://dx.doi.org/10.1080/00958970902846126

Journal of Coordination Chemistry
Vol. 62, No. 15, 10 August 2009, 2520–2531

Taylor & Francis
Taylor & Francis Group

Synthesis, crystal structure, and DNA binding of a new oxalato-bridged binuclear zinc(II) complex

WEI SUN, MAN JIANG, YAN-TUAN LI*,
ZHI-YONG WU and WEI-BING PENG

Marine Drug and Food Institute, Ocean University of China,
Qingdao, Shandong 266003, P.R. China

(*Received 27 October 2008; in final form 11 December 2008*)

A new binuclear zinc(II) complex bridged by μ-oxalate, and end-capped with 2,2′-bipyridine (bpy), $[Zn_2(ox)(bpy)_4](ClO_4)_2 \cdot H_2O$, has been synthesized and characterized by elemental analyses, molar conductance, IR, and electronic spectra and single-crystal X-ray diffraction. The single-crystal X-ray analysis reveals that the $[Zn_2(ox)(bpy)_4]^{2+}$ cation has two zinc(II) centers bridged by a planar bis(bidentate) oxalate group with Zn···Zn distance of 5.482(3) Å; each zinc(II) is in a distorted octahedral environment. The crystal structure is stabilized by non-classical C–H···O hydrogen bonds and π–π stacking interactions to form a 3-D supramolecular structure. The interaction of the complex with calf-thymus DNA (*CT*-DNA) was explored by using electronic and fluorescence spectra and viscosity measurements. The results reveal that the complex intercalates with *CT*-DNA with intrinsic binding constant of $4.1 \times 10^4\,M^{-1}$.

Keywords: μ-Oxalato-bridge; Dinuclear zinc(II) complex; Crystal structure; DNA interaction

1. Introduction

Interaction of metal complexes with parallel base-pairs of DNA is of interest [1–3]. Metal complexes can bind to DNA in non-covalent ways such as electrostatic, groove binding and intercalation [4, 5]. In particular, the intercalation of the metal complexes between parallel base-pairs of DNA is a binding mode between DNA and active anticancer drugs [6]. Intercalating ability correlates to the planarity of ligand and the coordination geometry of the metal ion [7, 8]. Relatively few studies on binuclear complexes have been reported to date [9–12]. However, interactions between binuclear complexes and DNA stimulate us to design and synthesize new binuclear complexes to evaluate and understand DNA binding and anticancer mechanism.

Oxalate is a versatile bridging ligand as bi-, tri-, or tetradentate capable of forming polynuclear complexes [13–15]. Several complexes bridged by oxalato have been synthesized and their magnetic properties were studied [16, 17]. However, to the best

*Corresponding author. Email: yantuanli@ouc.edu.cn

Journal of Coordination Chemistry
ISSN 0095-8972 print/ISSN 1029-0389 online
DOI: 10.1080/00958970902846126

of our knowledge, only five crystal structures of oxalato-bridged binuclear zinc(II) complexes have been characterized [Cambridge Structural Database (CSD), Version 5.28; Allen, 2002] [18], and none contains a polypyridyl ligand whose aromatic ring can offer the chance for its complex to bind DNA [19–21].

In this article, an oxalato-bridged binuclear zinc(II) complex $[Zn_2(ox)(bpy)_4](ClO_4)_2 \cdot H_2O$ was synthesized, structurally characterized by single crystal X-ray diffraction, and its DNA binding was studied.

2. Experimental

All reagents were of AR grade and used without purification. Calf-thymus DNA (*CT*-DNA) was purchased from Sigma Corp. and used as received. *N*,*N*′-*bis*[2-(dimethylamino)ethyl]oxamide (H_2dmaeoxd) was prepared according to the literature [22]. C, H, and N microanalyses were performed with a Perkin–Elmer 240 elemental analyzer. Molar conductance was measured with a Shanghai DDS-11A conductometer. Infrared spectrum was recorded with a Nicolet-470 spectrophotometer using a KBr pellet in the 4000–400 cm^{-1} region. Fluorescence was tested on a Fp-750w fluorometer equipped with quartz cuvettes of 1 cm path length at ambient temperature. The electronic spectrum was measured at room temperature on a Cary 300 spectrophotometer equipped with quartz cuvettes of 1 cm path length. Viscosity experiments were carried out using an Ubbelodhe viscometer maintained at 25.0 ± 0.1°C in a thermostatted water-bath.

Caution! Although we have not encountered any problems, perchlorate compounds are potentially explosive and should be handled with care.

2.1. *Preparation*

$[Zn_2(ox)(bpy)_4](ClO_4)_2 \cdot H_2O$ was obtained as follows: to a solution of H_2dmaeoxd (0.0230 g, 0.1 mmol) in methanol (10 mL) was added successively 0.2 mmol of piperidine and a solution of $Zn(ClO_4)_2 \cdot 6H_2O$ (0.0745 g, 0.2 mmol) in water (5 mL). After stirring for 20 min, bpy (0.0312 g, 0.2 mmol) in methanol (5 mL) was added. The reaction mixture was stirred at 333 K for further 2 h. Colorless crystals of the complex suitable for X-ray analysis were obtained from the solution by slow evaporation at room temperature after 2 days. Yield, 0.047 g (44%). Anal. Calcd for $Zn_2C_{42}H_{34}Cl_2N_8O_{13}$ (%): C, 47.57; H, 3.23; N, 10.57. Found: C, 47.49; H, 3.07; N, 10.59.

2.2. *Crystal structure determination*

The crystal structure analyses were carried out on a Bruker APEX area-detector diffractometer with graphite monochromated Mo-Kα radiation ($\lambda = 0.71073$ Å). The crystal structure was solved by the direct method followed by Fourier syntheses. Structure refinement was performed by full-matrix least-squares on F^2 using SHELXL-97 [23]. Water hydrogens were located in a difference Fourier map and included in the structure-factor calculation with fixed positional and isotropic displacement parameters [$U_{iso}(H) = 1.2U_{eq}(O)$]. Hydrogens on carbon were placed in calculated positions, with

Table 1. Crystal data and details of the structure determination.

Empirical formula	$Zn_2C_{42}H_{34}Cl_2N_8O_{13}$
Formula weight	1060.45
Crystal system	Triclinic
Space group	$P\bar{1}$
Units of cell dimensions (Å, °)	
a	11.572(5)
b	14.609(6)
c	14.799(6)
α	90.128(8)
β	111.273(7)
γ	102.444(7)
V (Å^3)	2267.7(16)
Z	2
D (Calcd) (g cm^{-1})	1.553
μ(Mo-Kα) (mm^{-1})	1.249
Scan-mode	φ and ω scan
F(000)	1080
Crystal size (mm^3)	$0.27 \times 0.23 \times 0.14$
θ range	2.0–25.0
Limiting indices	$-13 \le h \le 13$, $-17 \le k \le 1\ 4$, $-17 \le l \le 15$
Total unique data, $R_{(int)}$	11663, 7903, 0.074
Observed data [$I > 2\sigma(I)$]	2539
R, wR_2	0.0809, 0.2869
S	0.94
Maximum and minimum shift/error	0.000, 0.000

C–H distance of 0.93 Å, and refined as riding, with $U_{iso}(H) = 1.2U_{eq}(C)$. O12, O13, and O14 in perchlorate were disordered and were refined as two groups sharing the same Cl1 (occupancy factors are 0.6 and 0.4, respectively). For structure representations, Xp [24] and ORTEP-3 for windows [25] were used. Crystal data and refinement conditions are summarized in table 1.

2.3. *DNA-binding studies*

All experiments involving *CT*-DNA were performed in *Tris*-HCl buffer solution (pH = 7.86). Solutions of DNA in *Tris*-HCl gave a ratio of UV absorbance at 260 and 280 nm, A_{260}/A_{280}, of ≈1.9, indicating that the DNA was sufficiently free of protein [26]. The concentration of DNA was determined by UV absorbance at 260 nm. The extinction coefficient, ε260, was taken as 6600 L mol^{-1} cm^{-1} [27]. Stock solution of DNA was stored at 4°C and used after not more than 4 days. Concentrated stock solution of the zinc(II) complex was prepared by dissolving the complex in dimethyl sulfoxide (DMSO) and diluting with *Tris*-HCl buffer to required concentration.

Electronic spectral titration was performed by keeping the concentration of the complex constant while varying the *CT*-DNA concentration. Equal solution of DNA was added to the complex solution and reference solution to eliminate the absorbance of DNA itself. The fluorescence titration experiment was also performed by keeping the concentration of the complex constant while varying the DNA concentration and the spectra were obtained by using the excitation wavelength of 338 nm and an emission wavelength of 402 nm. In viscosity measurements, DNA samples approximately 200 base pairs in length were prepared by sonication in order to minimize complexities arising from DNA flexibility [28]. Flow times were measured with a digital stopwatch,

and each sample was measured three times, and an average flow time was calculated. Relative viscosities for DNA in the presence and absence of the complex were calculated from the relation $\eta = (t - t_0)/t_0$, where t is the observed flow time of DNA-containing solution and t_0 is that of *Tris*-HCl buffer alone. Data were presented as $(\eta/\eta_0)^{1/3}$ *versus* binding ratio [29], where η is the viscosity of DNA in the presence of complex and η is the viscosity of DNA alone.

3. Results and discussion

3.1. *Synthetic route and general properties of the binuclear complex*

The goal of this work was to prepare a dinuclear oxamidate complex of zinc(II), in which the oxamidate ligand (H_2dmaeoxd) has a bridging function and bpy is a terminal ligand. However, in the synthetic course of the complex, the oxalate-bridged binuclear zinc(II) complex, $[Zn_2(ox)(bpy)_4](ClO_4)_2 \cdot H_2O$, was obtained due to hydrolyzation of H_2dmaeoxd. The complex is sparsely soluble in water, ethanol, carbon tetrachloride, chloroform, and benzene, but soluble in DMF and DMSO to give stable solutions at room temperature. In the solid state the complex is fairly stable in air, facilitating physical measurements. The molar conductance values ($\Lambda = 167$ and $121\ \Omega^{-1}\,cm^2\,mol^{-1}$ in DMF and DMSO, respectively) of the binuclear zinc(II) complex fall in the expected range for 1 : 2 electrolytes [30], indicating that the two perchlorate anions are outside the metal coordination sphere, consistent with the IR data and crystal structure.

3.2. *IR and electronic spectra*

In the IR spectrum, a broad band centered at $3446\,cm^{-1}$ corresponds to ν(O–H) of water; the broadness is indicative of hydrogen bonds, consistent with the crystal structure [14]. The spectrum displays characteristic bands of the oxalate bridging ligand: ν_{as}(CO) at $1644\,cm^{-1}$ and ν_s(CO) at $1363\,cm^{-1}$ [31]. Bands of medium intensity, located in the 1610–1440 cm^{-1} region, are assigned to C–C and C–N stretching vibrations of coordinated bpy. The strong and broad band centered at $1093\,cm^{-1}$, and a strong sharp band at $623\,cm^{-1}$, indicate the presence of non-coordinated perchlorate [32]. The electronic spectrum of the complex was measured in the UV-Vis region (200–800 nm) in DMSO. Maxima were observed at 229 and 283 nm, due to π–π^* transitions of bpy. Further investigations of this and similar systems are required in order to obtain more detailed assignment for the charge transfer.

3.3. *Description of the crystal structure*

As shown in figure 1, the structure of $[Zn_2(ox)(bpy)_4](ClO_4)_2 \cdot H_2O$ consists of a non-centrosymmetric dinuclear $[Zn_2(ox)(bpy)_4]^{2+}$ cation and two uncoordinated ClO_4^- anions connected by a lattice water through O–H···O hydrogen bonds. Selected bond lengths and angles are listed in table 2. Due to the rigidity of the ligands, each hexacoordinated zinc(II) has a distorted octahedral geometry. The equatorial

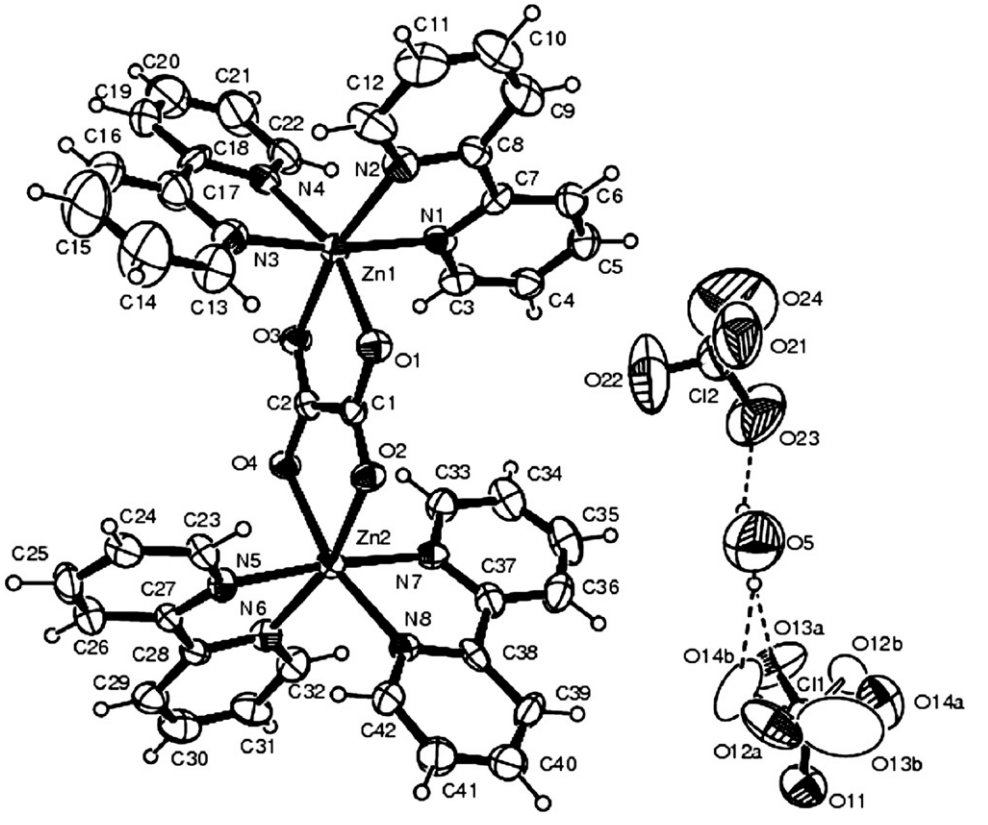

Figure 1. The molecular structure of the title complex, with 30% probability displacement ellipsoids. Dotted lines indicate hydrogen bonds.

coordination positions are occupied with two oxalate oxygens and two nitrogens of bpy [Zn–O distances range from 2.099(7) to 2.123(7) Å, while Zn–N distances range from 2.097(10) to 2.138(10) Å]. The axial positions are occupied by the other two nitrogens from each bpy ligand [Zn–N bond lengths in the 2.131(11)–2.186(10) Å range].

The deprotonated *bis*(bidentate) oxalate group is coordinated to two zinc(II)'s to form two, five-membered rings with 78.3(3)° and 78.5(3)° bite angles. The Zn1–Zn2 separation is 5.482(3) Å, which compares well with similar binuclear oxalate-bridged complexes [33, 34]. Within the oxalato bridge the C–O bonds have some double-bond character [1.224(12) to 1.261(12) Å], while the C1–C2 bond, 1.556(13) Å, is longer than that for a single bond (1.53 Å) [35]; these bonds are similar to those in many other oxalate complexes [36, 37]. The oxalate group is essentially planar [the largest deviation being 0.0029(6) Å at O4], Zn1 and Zn2 deviate from the plane by −0.124(10) and 0.232(10) Å, respectively.

The bpy ligands are bidentate, with bite angles from 75.2(4)° to 77.1(4)°. Each bpy mean plane is almost perpendicular to the oxalate bridge [the dihedral angles between bpy and oxalate bridge vary from 84.6(2)° to 88.0(2)°], while the dihedral angles between neighboring bpy mean planes are 75.2(2)° and 81.0(2)°.

In the crystal structure, the cations are stacked by face-to-face interactions among aromatic systems of bpy to form an infinite 3-D supramolecular network. As shown in

Table 2. Selected bond distances and angles (Å, °).

Zn1–O1	2.099(7)	Zn1–O3	2.116(7)
Zn1–N1	2.131(11)	Zn1–N2	2.139(10)
Zn1–N3	2.139(12)	Zn1–N4	2.103(11)
Zn2–O2	2.122(7)	Zn2–O4	2.111(7)
Zn2–N5	2.186(10)	Zn2–N6	2.123(9)
Zn2–N7	2.158(11)	Zn2–N8	2.097(10)
O1–C1	1.261(12)	O2–C1	1.224(12)
O3–C2	1.243(12)	O4–C2	1.240(12)
N1–C3	1.341(14)	C1–C2	1.556(13)
O1–Zn1–O3	78.3(3)	O1–Zn1–N1	92.3(3)
O1–Zn1–N2	94.4(3)	O1–Zn1–N3	92.3(4)
O1–Zn1–N4	160.2(3)	O3–Zn1–N1	93.4(3)
O3–Zn1–N2	167.1(4	O3–Zn1–N3	96.6(3)
O3–Zn1–N4	86.2(3)	N1–Zn1–N2	76.2(4)
N1–Zn1–N3	169.7(4)	N1–Zn1–N4	101.0(4)
N2–Zn1–N3	94.3(4)	N2–Zn1–N4	103.0(4)
N3–Zn1–N4	77.2(5)	O2–Zn2–O4	78.5(3)
O2–Zn2–N5	92.1(3)	O2–Zn2–N6	164.4(4)
O2–Zn2–N7	93.4(3)	O2–Zn2–N8	91.5(3)
O4–Zn2–N5	91.0(3)	O4–Zn2–N6	92.5(3)
O4–Zn2–N7	92.0(4)	O4–Zn2–N8	164.8(3)
N5–Zn2–N6	75.2(4)	N5–Zn2–N7	174.2(3)
N5–Zn2–N8	100.8(4)	N6–Zn2–N7	99.7(4)
N6–Zn2–N8	99.6(4)	N7–Zn2–N8	77.1(4)
O1–C1–O2	127.2(11)	O1–C1–C2	115.4(9)
O2–C1–C2	117.5(9)	O3–C2–C1	117.1(9)
O3–C2–O4	126.2(11)	O4–C2–C1	116.7(9)

figure 2, each cation interacts with five neighboring cations by π–π stackings with plane-to-plane separations of 3.417(14) [C6, $(-x, -y, 1-z)$] to 3.634(16) Å [C17, $(-x, -y, -z)$]. The bpy ligands also participate in non-classical C–H···O hydrogen bonds by acting as hydrogen-bond donors to O atoms of ox bridges and ClO_4^- (table 3). As shown in figure 3, $[Zn_2(ox)(bpy)_4]^{2+}$ units are assembled by two C–H···O hydrogen bonds to form a chain extending along the [1 1 1] direction. O12 and O14 of the perchlorate ion appear to be disordered and were refined as two groups [38]. If atoms O12–O14 adopt the A position, as shown in figure 4, each perchlorate interacts with four $[Zn_2(ox)(bpy)_4]^{2+}$ dications via four C–H···O hydrogen bonds to form a 2-D surpramolecular network parallel to (0 1 0) plane. If atoms O12–O14 adopt the B position, a 1-D chain extending along the [0 1 −1] direction is formed (figure 5).

3.4. *DNA-binding studies*

3.4.1. Fluorescence titration. Fluorescence titration has been widely used to characterize the interaction of complexes with DNA, by following the changes in fluorescence intensity of the complexes. The interaction between the complexes and *CT*-DNA can prevent fluorescence emission of the complexes from being quenched by polar solvent molecules and result in the enhancement of fluorescence intensity [39]. In the present investigation, it was used to monitor the interaction of the binuclear zinc(II) complex with DNA. As shown in figure 6, with the addition of increasing concentration of DNA, fluorescence intensity of the binuclear zinc(II) complex was

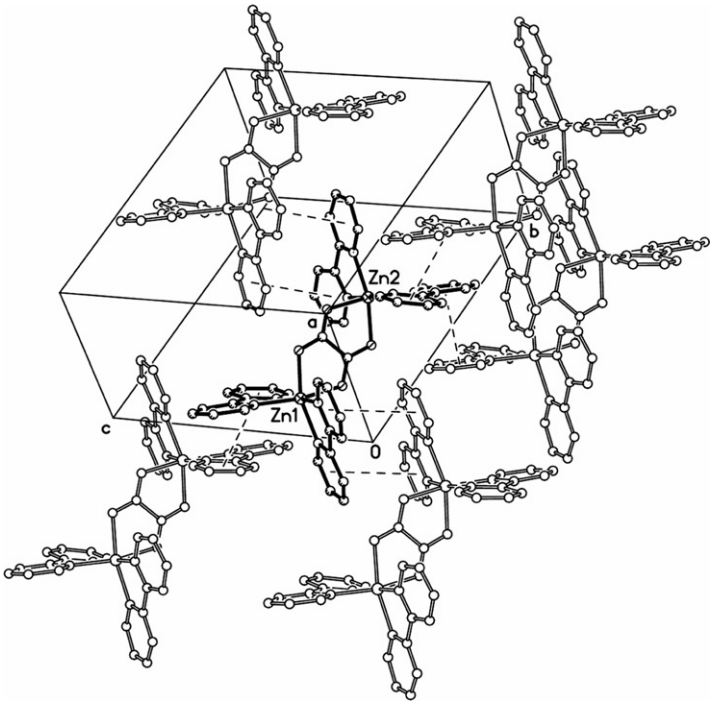

Figure 2. A packing diagram showing intermolecular π–π stacking between the bpy rings. All hydrogen atoms, water molecules, and ClO_4^- anions were omitted for clarity.

Table 3. Hydrogen-bond geometry (Å, °).

D–H···A	D–H	H···A	D···A	D–H···A
O5–H5A···O23	0.90	2.01	2.82(3)	150
O5–H5B···O13A	0.90	2.29	3.16(2)	162
O5–H5B···O14B	0.90	2.14	3.03(2)	167
C3–H3···O13A^{i}	0.93	2.48	3.25(3)	140
C9–H9···O11^{ii}	0.93	2.58	3.495(19)	169
C15–H15···O14A^{iii}	0.93	2.25	3.11(4)	153
C19–H19···O3^{iv}	0.93	2.51	3.273(17)	140
C24–H24···O14A^{v}	0.93	2.46	3.30(3)	150
C24–H24···O13B^{v}	0.93	2.55	3.14(3)	121
C30–H30···O12B^{vi}	0.93	2.52	3.18(2)	129
C32–H32···O23^{i}	0.93	2.57	3.36(2)	143
C39–H39···O2^{v}	0.93	2.47	3.223(14)	139

Symmetry codes: (i) $-x$, $1-y$, $1-z$; (ii) x, $y-1$, z; (iii) x, $y-1$, $z-1$; (iv) $-x$, $-y$, $-z$; (v) $1-x$, $1-y$, $1-z$; (vi) x, y, $z-1$.

enhanced substantially because of the protection of DNA. This implies that the binuclear zinc(II) complex interacts with, and is protected by, DNA.

3.4.2. Electronic absorption titration. To further investigate the interaction mode and strength between the binuclear zinc(II) complex and *CT*-DNA, the electronic absorption titration is also employed. Electronic absorption spectroscopy is an effective

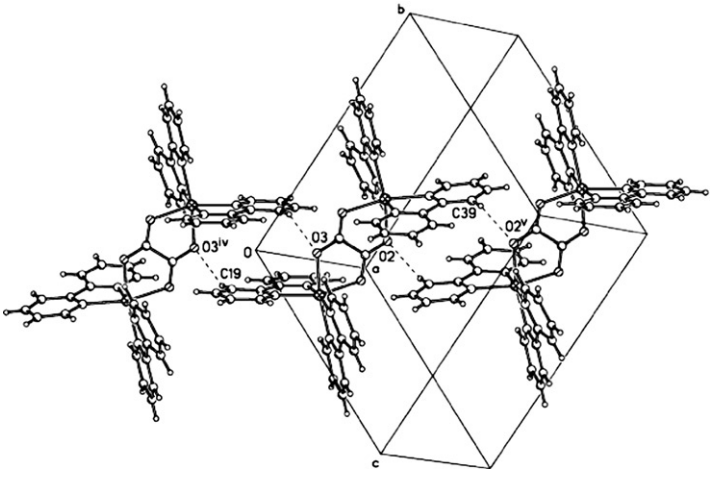

Figure 3. 1-D chain extending along the [1 1 1] direction. Water molecules and ClO_4^- anions were omitted for clarity. Symmetry codes: iv: $-x, -y, -z$; v: $1-x, 1-y, 1-z$.

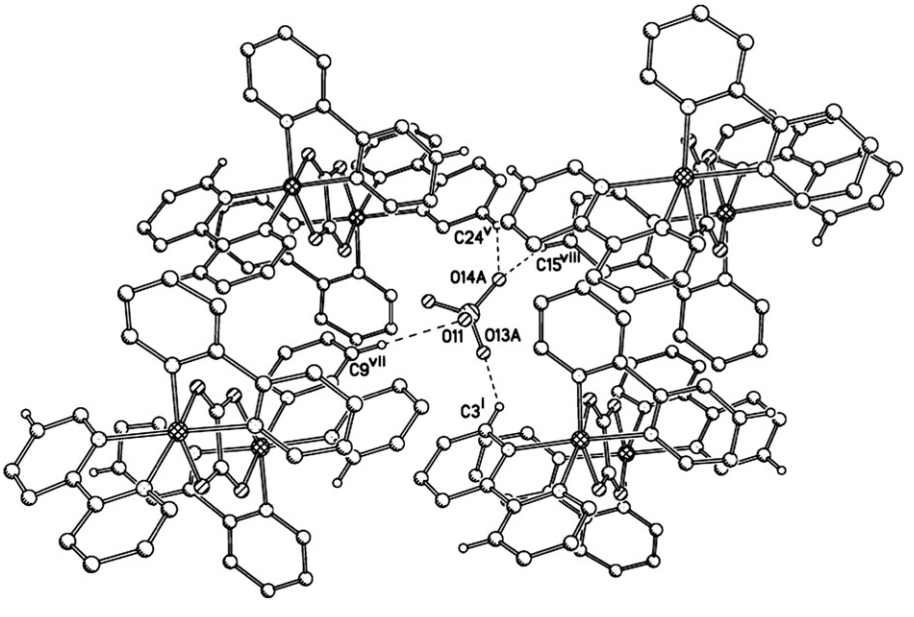

Figure 4. The hydrogen-bonding interactions, viewed down the *b*-axis. Atoms O12B–O14B, H-atoms not involved in hydrogen-bonding, water molecules, and ClO_4^- anion (Cl2) were omitted for clarity. Symmetry codes: i: $-x, 1-y, 1-z$; v: $1-x, 1-y, 1-z$; vii: $x, 1+y, z$; viii: $x, 1+y, 1+z$.

method to examine the binding modes and binding extent of metal complexes with DNA [40]. Hypochromism and red shift are associated with binding of metal complexes to the DNA helix, due to intercalation involving a strong stacking interaction between the aromatic chromophore of complexes and the base pairs of DNA.

As shown in figure 7, titration of *CT*-DNA into the complex caused spectral changes. The π–π^* transition of the binuclear zinc(II) complex, observed at 283 nm, exhibits hypochromism of about 13.4% with slight red shifts of 2 nm at a ratio of [DNA]/

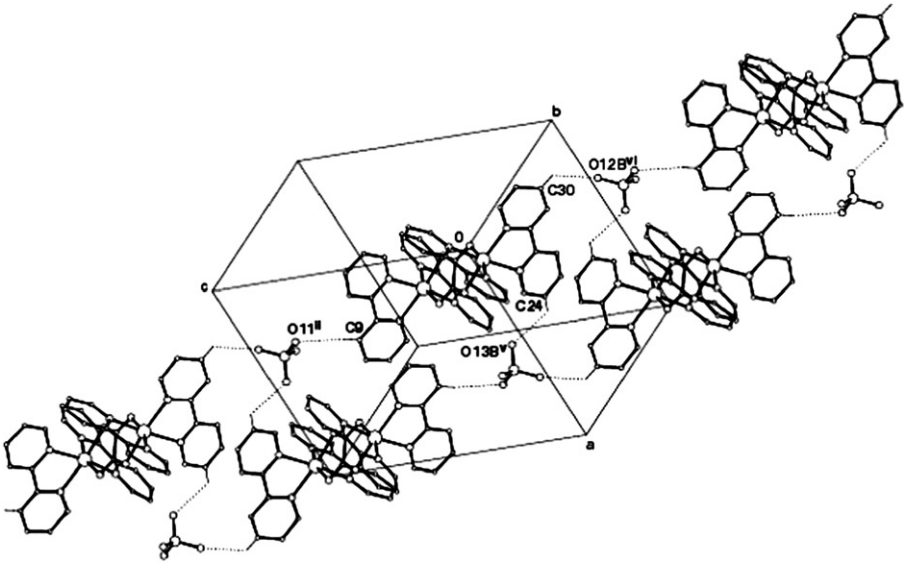

Figure 5. 1-D chain extending along the [0 1 −1] direction. Atoms O12A–O14A, H-atoms not involved in hydrogen-bonding, water molecules, and ClO_4^- anion (Cl2) were omitted for clarity. Symmetry codes: ii: $x, y-1, z$; v: $1-x, 1-y, 1-z$; vi: $x, y, z-1$.

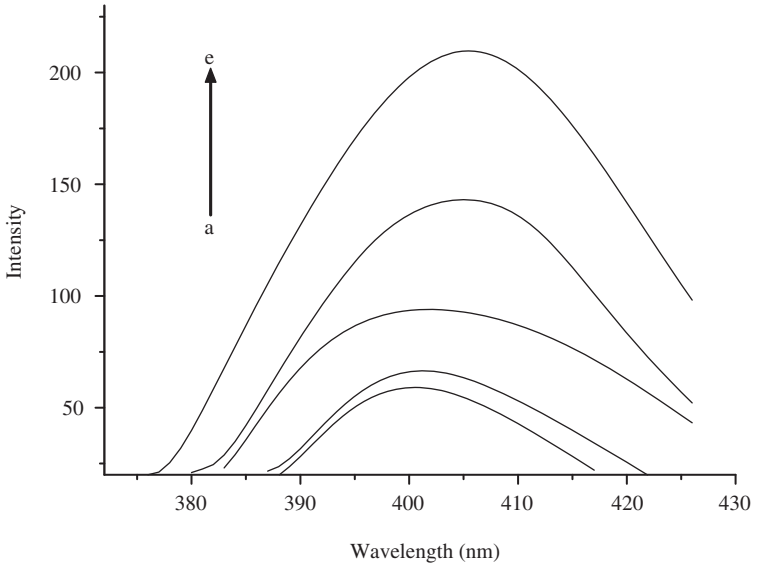

Figure 6. Fluorescence changes that occur when the complex is titrated with *CT*-DNA: $\lambda_{ex} = 338$ nm; [complex] $= 2.4 \times 10^{-5}$ mol L^{-1}; and [DNA] = (a) 0, (b) 3.0×10^{-5}, (c) 6.0×10^{-5}, (d) 9.0×10^{-5}, and (e) 12.0×10^{-5} mol L^{-1}. The arrow shows the intensity change upon increasing DNA concentration.

[complex] of 9. Obviously, these spectral characteristics suggest that the complex interacts with DNA most likely through intercalation with π–π stacking between the aromatic chromophore and the base pairs of DNA. When the complex intercalates the base pairs of *CT*-DNA, the π^* orbital of the intercalated ligand (bpy) can couple with

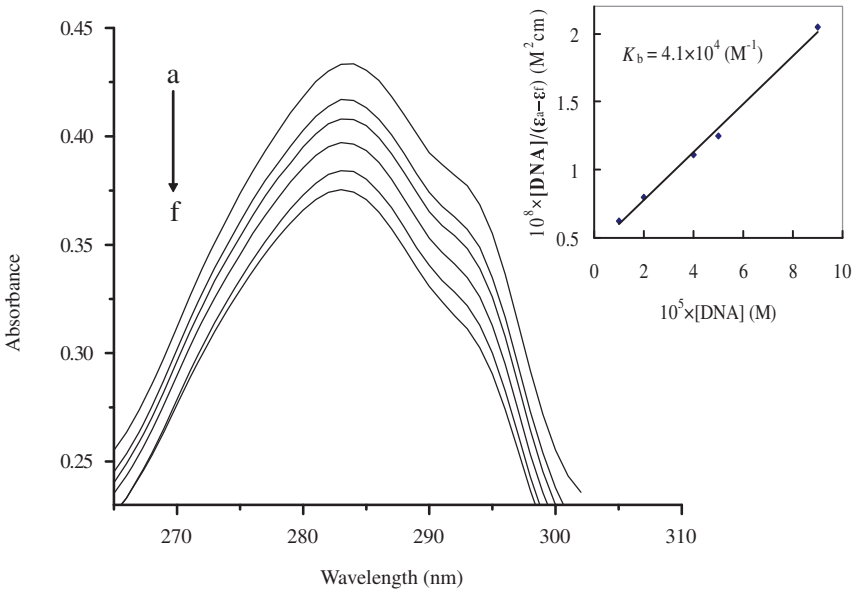

Figure 7. Absorption spectra of $[Zn_2(ox)(bpy)_4](ClO_4)_2 \cdot H_2O$ in the presence of *CT*-DNA at different concentrations. [Complex] = 10^{-5} mol L^{-1} and [DNA] = (a) 0, (b) 10^{-5}, (c) 2×10^{-5}, (d) 4×10^{-5}, (e) 5×10^{-5}, and (f) 9×10^{-5} mol L^{-1}. The arrow shows the intensity change upon increasing DNA concentration. Insert: Plot of [DNA]/($\varepsilon_a - \varepsilon_f$) vs. [DNA] for the titration of DNA with the complex.

the π orbital of the base pair, decreasing the π–π^* transition energy and resulting in the bathochromism. Furthermore, the coupling π-orbital is partially filled by electrons, thus decreasing transition probabilities and concomitantly resulting in hypochromism.

In order to quantify the affinity of the complex towards *CT*-DNA, the intrinsic binding constant of the complex, K_b, was determined from the spectral titration data using equation [41]:

$$[DNA]/(\varepsilon_a - \varepsilon_f) = [DNA]/(\varepsilon_b - \varepsilon_f) + 1/K_b(\varepsilon_b - \varepsilon_f)$$

where ε_a, ε_f, and ε_b correspond to the extinction coefficient, respectively, for each addition of *CT*-DNA to the zinc(II) complex, for the free zinc(II) complex and for the zinc(II) complex in the fully bound form. In the plot of [DNA]/($\varepsilon_a - \varepsilon_f$) *versus* [DNA] (figure 4), K_b is given by the ratio of the slope to intercept ($K_b = 4.1 \times 10^4\,M^{-1}$, $R^2 = 0.9896$ for five points). The K_b value of the complex compares well with those of the well-established intercalation agents $[Co(bpy)_2(CNOIP)]^{3+}$ (CNOIP = 2-(2-chloro-5-nitrophenyl)imidazo-[4, 5-*f*][1,10]phenanthroline) ($K_b = 5.0 \times 10^4\,M^{-1}$) [42] and $[Ru(tpy)(PPh_3)_2Cl]^+$ (tpy = 2, 2′ : 6′, 2″-terpyridine) ($K_b = 4.1 \times 10^4\,M^{-1}$) [43].

3.4.3. Viscosity measurement. Although spectral methods are necessary, they are not sufficient to determine a binding mode. In order to clarify the interaction between complex and *CT*-DNA, viscosity was carried out. In classical intercalation the DNA helix lengthens as base pairs are separated to accommodate the bound ligand leading to increased DNA viscosity, whereas in groove binding and electrostatic mode the length of the helix is unchanged with no apparent alteration in DNA viscosity [44].

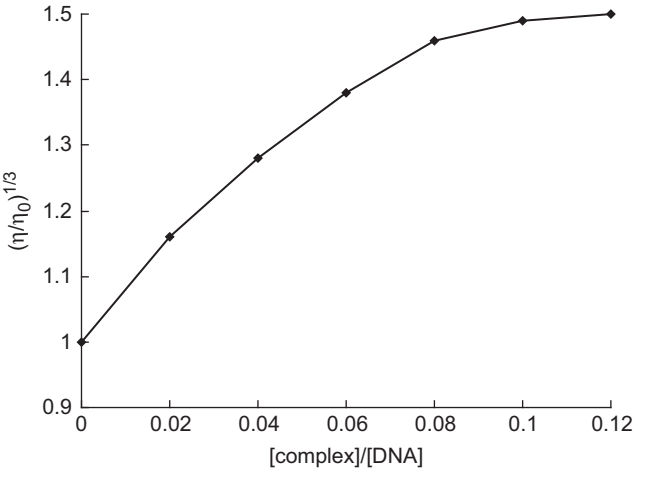

Figure 8. Effect of increasing amounts of binuclear zinc(II) complex on the relative viscosity of *CT*-DNA at 25.0 ± 0.1°C.

Therefore, viscosity is regarded as the least ambiguous and the most critical means for studying the binding mode of metal complexes with DNA [44, 45].

The binuclear zinc(II) complex increases (figure 8) the relative viscosity of *CT*-DNA with increasing concentration of the zinc(II) complex, consistent with intercalation. Thus, the results obtained from viscosity studies validate those obtained from UV-Vis spectral titration and fluorescence spectra. Further investigations on this and similar systems are still required to get deeper insight into DNA binding with oxalato-bridged complexes and are in progress in our laboratory.

Supplementary materials

Crystallographic data (excluding structure factors) for the structure reported in this work has been deposited with the Cambridge Crystallographic Data Center and allocated the deposition number: 634802.

Acknowledgments

This project was supported by the National Natural Science Foundation of China (No. 30672515), the PhD Program Foundation of Ministry of Education of China (No. 20060423005), and the National Undergraduate Innovative Test Program of China (No. 2007SR25).

References

[1] H.X. Zhang, B.S. Kang, A.W. Xu, Z.N. Chen, Z.Y. Zhou, A.S.C. Chan, K.B. Yu, C. Ren. *J. Chem. Soc., Dalton Trans.*, 2559 (2001).

[2] Y. Qu, A. Harris, A. Hegmans, A. Petz, P. Kabolizadeh, H. Penazova, N. Farrell. *J. Inorg. Biochem.*, **98**, 1591 (2004).
[3] M. Mounir, J. Lorenzo, M. Ferrer, M.J. Prieto, O. Rossell, F.X. Avilès, V. Moreno. *J. Inorg. Biochem.*, **101**, 660 (2007).
[4] C.Y. Zhou, J. Zhao, Y.B. Wu, C.X. Yin, Y. Pin. *J. Inorg. Biochem.*, **101**, 10 (2007).
[5] F. Gao, H. Chao, F. Zhou, Y.X. Yuan, B. Peng, L.N. Ji. *J. Inorg. Biochem.*, **100**, 1487 (2006).
[6] K.E. Erkkila, D.T. Odom, J.K. Barton. *Chem. Rev.*, **99**, 2777 (1999).
[7] H. Xu, K.C. Zheng, Y. Chen, Y.Z. Li, L.J. Lin, H. Li, P.X. Zhang, L.N. Ji. *Dalton Trans.*, 2260 (2003).
[8] H. Xu, K.C. Zheng, H. Deng, L.J. Lin, Q.L. Zhang, L.N. Ji. *New J. Chem.*, **27**, 1255 (2003).
[9] Y. Li, Y. Wu, J. Zhao, P. Yang. *J. Inorg. Biochem.*, **101**, 283 (2007).
[10] Q.Q. Zhang, F. Zhang, W.G. Wang, X.L. Wang. *J. Inorg. Biochem.*, **100**, 1344 (2006).
[11] F. Zhang, Q.Q. Zhang, W.G. Wang, X.L. Wang. *J. Photochem. Photobiol., A*, **184**, 241 (2006).
[12] H. Ojima, K. Nonoyama. *Coord. Chem. Rev.*, **92**, 85 (1988).
[13] H.Y. Shen, W.M. Bu, D.Z. Liao, Z.H. Jiang, S.P. Yan, G.L. Wang. *Inorg. Chem.*, **39**, 2239 (2000).
[14] O. Castillo, A. Luque, P. Román. *J. Mol. Struct.*, **570**, 181 (2001).
[15] S.H. Wang, Y.T. Li, C.W. Yan. *Polish J. Chem.*, **80**, 865 (2006).
[16] I. Muga, J.M. Gutierrez-Zorrilla, P. Vitoria, A. Luque, M. Insausti, P. Roman, F. Lloret. *Eur. J. Inorg. Chem.*, 2541 (2000).
[17] Y. Akhriff, J. Server-Carrió, A. Sancho, J. García-Lozano, E. Escrivá, J.V. Folgado, L. Soto. *Inorg. Chem.*, **38**, 1174 (1999).
[18] J.P. Zhang, Y.Y. Lin, X.C. Huang, X.M. Chen. *Eur. J. Inorg. Chem.*, 3407 (2006).
[19] R.E. Holmlin, J.A. Yao, J.K. Barton. *Inorg. Chem.*, **38**, 174 (1999).
[20] Q.L. Zhang, J.G. Liu, H. Xu, H. Li, J.Z. Liu, H. Zhou, L.H. Qu, L.N. Ji. *Polyhedron*, **20**, 3049 (2001).
[21] R. Indumathy, S. Radhika, M. Kanthimathi, T. Weyhermuller, B.U. Nair. *J. Inorg. Biochem.*, **101**, 434 (2007).
[22] H. Ojima, Y. Yamada. *Bull. Chem. Soc. Jpn.*, **43**, 3018 (1970).
[23] G.M. Sheldrick. *SHELXL-97, Program for Crystal Structure Refinement*, University of Göttingen, Germany (1997).
[24] Siemens. *XP. Version 5.03, Siemens Analytical X-ray Instruments Inc.*, Madison, Wisconsin, USA (1994).
[25] L.J. Farrugia. ORTEP3 for Windows, Program for Drawing Thermal Ellipsoid Plot. *J. Appl. Cryst.*, **30**, 565 (1997).
[26] J. Marmur. *J. Mol. Biol.*, **3**, 208 (1961).
[27] M.E. Reichmann, S.A. Rice, C.A. Thomas, P.J. Doty. *J. Am. Chem. Soc.*, **76**, 3047 (1954).
[28] G. Cohen, H. Eisenberg. *Biopolymers*, **8**, 45 (1969).
[29] J.K. Barton, J.M. Goldberg, C.V. Kumar, N.J. Turro. *J. Am. Chem. Soc.*, **108**, 2081 (1986).
[30] W.J. Geary. *Coord. Chem. Rev.*, **7**, 81 (1971).
[31] R. Cortés, M.K. Urtiaga, L. Lezama, M.I. Arriortua, T.A. Rojo. *Inorg. Chem.*, **33**, 829 (1994).
[32] W. Radecka-Paryzek. *Inorg. Chim. Acta*, **34**, 5 (1979).
[33] H. Jo, A.J. Lough, J.C. Kim. *Inorg. Chim. Acta*, **358**, 1274 (2005).
[34] R. Vaidhyanathan, S. Natarajan, C.N.R. Rao. *J. Chem. Soc., Dalton Trans.*, 699 (2001).
[35] F.H. Allen, O. Kennard, D.G. Watson, L. Brammer, A.G. Orpen, R. Taylor. *J. Chem. Soc., Perkin Trans. II*, S1 (1987).
[36] S. Triki, F. Bérézovsky, J.S. Pala, E. Coronado, C.J. Gómez-García, J.M. Clemente, A. Riou, P. Molinié. *Inorg. Chem.*, **39**, 3771 (2000).
[37] J. Lu, K. Zhao, Q.R. Fang, J.Q. Xu, J.H. Yu, X. Zhang, H.Y. Bie, T.G. Wang. *Cryst. Growth Des.*, **5**, 1091 (2005).
[38] W. Sun, Y.T. Li, Z.Y. Wu, J.L. Liu. *Acta Cryst.*, **C63**, m462 (2007).
[39] J.H. Zhou, S.Q. Xia, J.R. Chen. *J. Photochem. Photobiol., A*, **165**, 143 (2004).
[40] A. Wolfe, G.H. Shimer Jr, T. Meehan. *Biochemistry*, **26**, 6392 (1987).
[41] A.M. Pyle, J.P. Rehmann, R. Meshoyrer, C.V. Kumar, N.J. Turro, J.K. Barton. *J. Am. Chem. Soc.*, **111**, 3051 (1989).
[42] Q.L. Zhang, J.G. Liu, J. Liu, G.Q. Xue, H. Li, J.Z. Liu, H. Zhou, L.H. Qu, L.N. Ji. *J. Inorg. Biochem.*, **85**, 291 (2001).
[43] S. Sharma, S.K. Singh, M. Chandra, D.S. Pandey. *J. Inorg. Biochem.*, **99**, 458 (2005).
[44] S. Satyanarayana, J.C. Dabrowiak, J.B. Chaires. *Biochemistry*, **32**, 2573 (1993).
[45] S. Satyanarayana, J.C. Dabrowiak, J.B. Chaires. *Biochemistry*, **31**, 9319 (1992).